MUCH: An Imaging Čerenkov Telescope for Volcano Muography

D. Mollica,[1] O. Catalano,[1] M. Capalbi,[1] G. Contino,[1] P. Conconi,[2] G. Cusumano,[1] F. D'Anca,[3] M. Del Santo,[1] C. Gargano,[1] V. La Parola,[1] G. La Rosa,[1] M. C. Maccarone,[1] T. Mineo,[1] G. Pareschi,[2] and G. Sottile[1]

[1]*INA-Istituto di Astrofisica Spaziale e Fisica Cosmica di Palermo, Via U. La Malfa 153, 90146 Palermo, Italy*

[2]*INA-Osservatorio Astronomico di Brera, Via E. Bianchi 46, 23807 Merate, Italy*

[3]*INAF-Osservatorio Astronomico di Palermo, Piazza del Parlamento 1, 90134 Palermo, Italy*

Corresponding author: D. Mollica
Email: davide.mollica@inaf.it

Abstract

In the last decades, several attempts have been made to investigate internal structures of large bodies, such as volcanoes, with transmission muography. High spatial resolution and reduction of the strong background noise, due to protons, electrons, and scattered low-energy muons, are the main challenges for this technique. As a possible solution to fulfill these requirements, muography with Imaging Atmospheric Čerenkov Telescopes (IACTs) has been recently proposed and the feasibility demonstrated by our team using GEANT4 simulations. IACTs are telescopes dedicated to gamma-ray astronomy consisting of an optical system that focuses the Čerenkov light into a high-sensitive and fast read-out camera. Muons with energy above about 5 GeV induce Čerenkov radiation which is emitted in a cone with a constant opening angle around their travel direction. As IACTs image in angular space, the Čerenkov light focused onto the camera forms a ring-shaped image centered at a distance from the focal plane center proportional to the muon incidence angle. None of the previously mentioned sources of background is expected to affect the IACTs muon signal. Here, we present MUCH, a lightweight and compact IACT design, specifically dedicated to volcano muography. The telescope design is based on a SiPMs camera working in the 280 nm–900 nm wavelength band, equipped with fast readout electronics with single-photon counting capability. The proposed Schmidt-like optical system is composed of a 2.5 m aspherical mirror and a 2.5 m PMMA Fresnel lens corrector. It results in a field of view of about 12°, an entrance pupil of 2.5 m diameter, and an angular resolution better than 0.2° throughout the entire FoV which allows us to determine the muon direction with a reconstruction precision better than a few tenths of a degree. A Geant4 framework for the simulation of Fresnel lenses and aspherical mirrors is currently being developed for the telescope prototype achievement.

Keywords: muography, Geant4, imaging atmospheric Čerenkov telescope, RADIOROC
DOI: 10.31526/JAIS.2022.255

1. INTRODUCTION

Particles seen by current muon telescopes are not only muons coming from the target. Indeed, muography can be affected by a huge particle background [1, 2, 3, 4] due to scattered low energy muons, charged particles from Extensive Air Showers (EASs), random coincidences of different particles, and upward-going particles entering the back of the detector. The latter background source can be reduced by time-of-flight techniques that require a sub-ns time resolution readout system [5, 6]. The EAS particles and soft-muons components of the background can be reduced by increasing the number of detector planes and using lead walls to discriminate low-energy particles [7, 8]. This solution increases the weight and dimensions of the instrument, limiting its portability. In order to overcome this problem, muography with Imaging Atmospheric Čerenkov Telescopes (IACTs) has been recently proposed [9, 10]. This technique exploits the induced Čerenkov radiation along the muon trajectory. Although IACTs can observe only at night, none of the previously mentioned sources of background is expected to affect the observed muon flux. Indeed, Čerenkov radiation is induced only by muons with kinetic energy greater than about 4.5 GeV, so low-energy muons are not detected.

The feasibility of muography with IACTs has been demonstrated by our team using GEANT4 simulations for muon transportation and the ASTRI-Horn telescope[1] simulator for optical ray tracing [11]. Simulation results of the muography of a volcano toy model have shown an angular resolution better than a few tenths of a degree and a muon collection area greater than the telescope aperture area.

[1] http://www.ifc.inaf.it/index.php/projects/the-astri-telescopes/

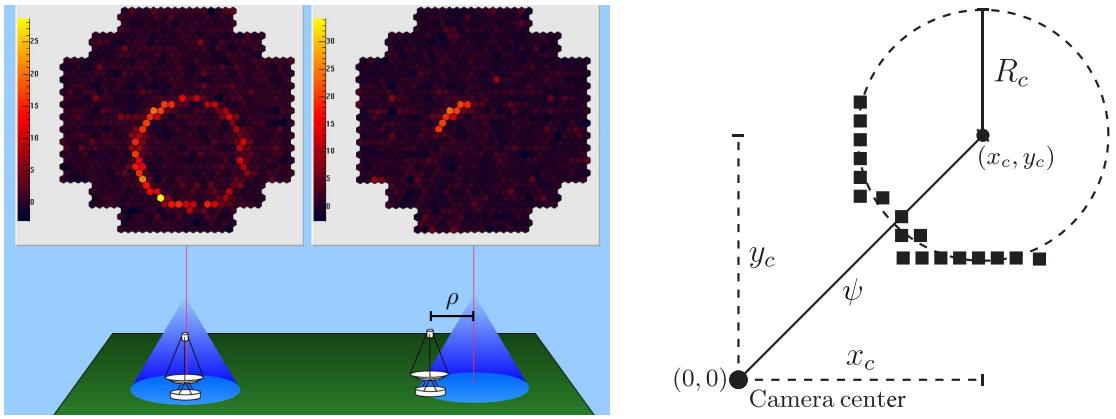

(a) (b)

FIGURE 1: (a) Muons hitting an IACT aperture plane in the center and at a distance ρ (credit: [13]). When the muon passes through the telescope aperture, the ring appears complete; otherwise, its angular extent decreases with increasing ρ. (b) Reconstruction of muon direction and Čerenkov angle from radius and center of an IACT muon image.

2. MUON DETECTION WITH IACTS

A charged particle induces Čerenkov radiation when it passes through a refractive medium at a speed greater than the speed of light in that medium. Photons of energy ϵ are emitted with an angle θ_c, relative to the particle direction, which depends on the particle speed βc_0, where c_0 is the speed of light in vacuum, and on the medium refractive index $n(\epsilon)$:

$$\theta_c = \arccos \frac{1}{\beta n(\epsilon)}. \tag{1}$$

For muons in the atmosphere at sea level, this implies a process energy threshold of about 4.5 GeV and a limit on Čerenkov angle of about 1.4°. The energy spectrum of the emitted photons per unit path length is given by the Frank-Tamm formula

$$\frac{\mathrm{d}N}{\mathrm{d}\epsilon \mathrm{d}z} = \frac{\alpha}{\hbar c_0}\left(1 - \frac{1}{\beta_\mu^2 n^2(\epsilon)}\right), \tag{2}$$

where α is the fine-structure constant and $\hbar$ is the reduced Planck constant.

Consider a muon passing near an IACT with a track, nearly parallel to the optical axis, which intersects the telescope aperture plane at a distance ρ (the *impact parameter*) from the aperture center (see Figure 1(a)). The induced Čerenkov photons do not cover the telescope aperture plane uniformly. Indeed, the radial distribution of photons has inverse-distance dependence from the impact point

$$\sigma_{\mathrm{ph}}(r) \propto \frac{1}{r}. \tag{3}$$

As a consequence, at fixed ρ/R_a, the number of Čerenkov photons reaching the telescope aperture is not proportional to the telescope aperture area but to its aperture radius R_a. With a 2.5 m telescope aperture, only the photons emitted in about the last 100 m can be seen, resulting in a signal of few ns. The number of photons on the aperture decreases with the impact parameter; a minimum of about 1000 photons and a maximum of about 3000 photons are expected for $\rho < 2$ m.

As IACTs image in angular space, the Čerenkov light focused onto the camera forms a ring-shaped image centered at a distance from the focal plane center corresponding to the angle of incidence of the muon and with an angular extent ϕ_{ext} that decreases as the impact parameter increases [12]:

$$\phi_{\mathrm{ext}} = \begin{cases} 2\pi & \text{if } \rho < R_a, \\ 2\arcsin\left(\frac{R_a}{\rho}\right) & \text{if } \rho \geq R_a. \end{cases} \tag{4}$$

After a cleaning procedure on the image, the muon arrival direction (the ring center) with respect to the telescope axis can be measured with a mere geometrical analysis (see Figure 1(b)). In addition, from the ring radius, one can infer the muon energy up to about 20 GeV; above this energy, the Čerenkov angle saturates at about 1.4° at sea level.

3. OPTICAL AND DETECTION SYSTEM OF THE MUCH TELESCOPE

3.1. Telescope Design

The MUCH optical system is derived from the Schmidt telescope configuration. It utilizes a Schmidt corrector plate and a primary mirror as in the conventional Schmidt configuration, but

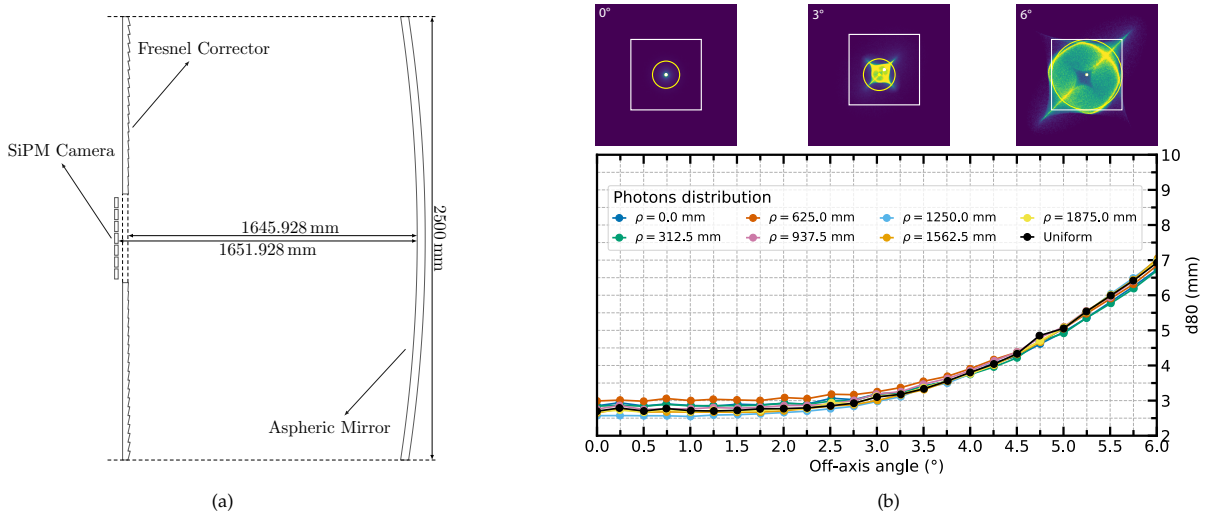

(a) (b)

FIGURE 2: (a) Sketch of the optical system of MUCH. (b), (Above) Optical system spot diagram at 0°, 3°, and 6° off-axis angle. The white box is 7 mm × 7 mm. (Below) 80% encircled photons diameter (d80) as a function of off-axis angle and with different photons distributions on the aperture: uniform and induced by muons with different ρ. Simulations have been performed with a dedicated GEANT4 simulator.

TABLE 1: MUCH lens and mirror profile parameters.

Parameter	Fresnel lens	Aspherical mirror
R	1250 mm	1250 mm
$1/c$	−7332.285 mm	−3784.375 mm
k	0.0	0.0
α_1	0.0	0.0
α_2	$2.176\,931\,7 \times 10^{-11}$	$-4.396\,288\,9 \times 10^{-12}$
α_3	$5.141\,933\,8 \times 10^{-19}$	$1.769\,375\,7 \times 10^{-19}$
α_4	$1.103\,78 \times 10^{-24}$	$-1.295\,832\,8 \times 10^{-25}$

TABLE 2: MUCH optical system main parameters.

Parameter	Value
Effective focal length	1854.66 mm
Entrance pupil diameter	2500 mm
$f/\#$	0.74
Plate scale	32.37 mm/°
Mirror diameter	2500 mm
Corrector diameter	2500 mm
Corrector central window side	420 mm
Focal plane side	420 mm
Corrector-mirror distance	1645.93 mm
Back focal length	1651.93 mm

(i) the corrector is implemented as a 5 mm thin Fresnel lens,

(ii) the corrector is placed at the focal point of the mirror instead of at its center of curvature,

(iii) the mirror profile is aspherical instead of spherical.

Furthermore, the optical system focal surface results flattened. The position of the corrector yields to a very compact configuration and to an easy-to-manufacture flat focal surface, but at the expense of the simplicity of the mirror optical surface. In order to reduce the optical aberration across the field of view, the telescope lens and mirror design has been optimized with Zemax OpticStudio[2]. The optical surfaces sagitta of the system is described by the equation

$$s(r) = \frac{cr^2}{1+\sqrt{1-c^2r^2(1+k)}} + \sum_{i=1} \alpha_i r^{2i}, \tag{5}$$

where c is the lens curvature, k is the conic constant, and α_i are the aspheric constants. The optimized profile parameters are listed in Table 1. The diameter of both corrector and mirror is 2500 mm, and the axial distance between them is 1645.93 mm. The effective focal length of the system is 1854.66 mm, and the telescope plate scale is 32.37 mm/°. These and other parameters of the optical design are summarized in Table 2. The distance between the mirror and the focal plane is 1651.93 mm. The focal plane is covered by a matrix of 7 × 7 PDMs, each one composed of a matrix of 8 × 8 SiPMs sensor with a 6.95 mm × 6.95 mm active area working in the 280 nm–900 nm wavelength band, so the pixel angular size is 0.22° × 0.22°.

[2] https://www.zemax.com/products/opticstudio

Electronics. An innovative fast front-end electronics will be used for the SiPMs readout. The Application-Specific Integrated Circuit (ASIC) designed, the RADIOROC (RADIOgraphy Read Out Chip) [14], is an improvement of an existing ASIC, used in the ASTRI-Horn project. RADIOROC is able to operate SiPMs both in charge integration and in single-photon counting (150 MHz). The latter is essential for acquiring the very brief in time (few ns) muon signal minimizing the night sky background.

3.2. GEANT4 *Simulation Results*

3.2.1. MUCH Simulator

In order to simulate a telescope that combines Fresnel lenses and aspherical mirrors, a dedicated GEANT4 simulation framework is currently being developed. The purpose is to provide a flexible module for the creation of Fresnel lenses, mirrors, and SiPM cameras reducing the complexity of GEANT4 geometry description and simplifying the implementation of materials optical properties. The framework main classes are as follows:

(i) `MuchFresnelLens` class, which allows for the creation of customizable Fresnel lenses,

(ii) `MuchStandardLens` class, which allows for the creation of customizable "aspherical shell" solids,

(iii) `MuchCamera` class, which allows for the creation of customizable SiPM cameras.

3.2.2. Optical Performance Simulations

As already mentioned in Section 2, Čerenkov photons induced by muons are not uniformly distributed on the telescope aperture plane. Since the optical performance depends on both photon incidence angle and incidence position on the corrector, simulations with muon-induced photon distribution have been performed. To simplify the characterization of the telescope optical performance as a function of the sole impact parameter ρ, we derived, using equation (3), a photon distribution induced by muons uniformly distributed over a thin ring of radius ρ:

$$\sigma_{\mathrm{ph}}(r,\rho) \propto \frac{1}{|r-\rho|} K\left(-\frac{4r\rho}{(r-\rho)^2}\right), \tag{6}$$

where r is the distance from the impact point and K is the complete elliptic integral of the first kind. Using such photon distribution, the derived optical performance descriptors are averaged over muon impact azimuth angle and depend only on ρ. Moreover, the photon spectrum used in the simulations is the convolution of the Čerenkov spectrum (2) with the SiPM photon detection efficiency.

Simulation results are shown in Figure 2(b). The diameter, d80, of the smallest circle that encircles the 80% of photons focused on the focal plane has been used to characterize the system performance. The polychromatic d80 is below the dimension of a SiPM pixel up to 6° off-axis. It is worth noting that the d80 depends only slightly on the muon impact parameter, which means that the system response is uniform over the whole aperture.

4. CONCLUSION

Muography with IACTs is a novel promising technique that exploits the muon-induced Čerenkov radiation in the atmosphere in order to perform muon detection. Due to IACT image capability and high Čerenkov energy threshold, negligible background, muon collection area greater than the telescope aperture, and an angular resolution better than a few tenths of a degree are expected.

MUCH, a compact Schmidt-like IACT designed for muography, has been presented. The design provides an angular resolution better than 0.22° (pixel angular size) over the entire FoV of 12°. The SiPM camera will be equipped with a new fast front-end electronics able to acquire the muon Čerenkov flash minimizing optical background signals. An international patent has been registered (PCT/IB2016/056937).

CONFLICTS OF INTEREST

The authors declare that there are no conflicts of interest regarding the publication of this paper.

References

[1] J. Peña Rodríguez, H. Asorey, and L. Alberto Núñez. Characterization of the muography background using the Muon Telescope (MuTe). `https://ui.adsabs.harvard.edu/abs/2021chep.confE.984P`, Apr 2021.

[2] Kanetada Nagamine. Introductory muon science. `https://doi.org/10.1017/CBO9780511470776`, 2003.

[3] R. Nishiyama, S. Miyamoto, and N. Naganawa. Experimental study of source of background noise in muon radiography using emulsion film detectors. `https://gi.copernicus.org/articles/3/29/2014/`, 2014.

[4] H. Gómez, D. Gibert, C. Goy, K. Jourde, Y. Karyotakis, S. Katsanevas, J. Marteau, M. Rosas-Carbajal, and A. Tonazzo. Forward scattering effects on muon imaging. `https://doi.org/10.1088/1748-0221/12/12/p12018`, Dec 2017.

[5] Jacques Marteau, Jean de Bremond d'Ars, Dominique Gibert, Kevin Jourde, Serge Gardien, Claude Girerd, and Jean-Christophe Ianigro. Implementation of sub-nanosecond time-to-digital convertor in field-programmable gate array: applications to time-of-flight analysis in muon radiography. `https://doi.org/10.1088/0957-0233/25/3/035101`, Feb 2014.

[6] L. Cimmino, F. Ambrosino, L. Bonechi, R. Ciaranfi, R. D'Alessandro, V. Masone, N. Mori, P. Noli, G. Saracino, and P. Strolin. The MURAVES telescope front-end electronics and data acquisition. `https://doi.org/10.4401/ag-7379`, Feb 2017.

[7] László Oláh, Hiroyuki K. M. Tanaka, Takao Ohminato, and Dezső Varga. High-definition and low-noise muography of the sakurajima volcano with gaseous tracking detectors. https://doi.org/10.1038/s41598-018-21423-9, Feb 2018.

[8] Raffaello D'Alessandro, F. Ambrosino, G. Baccani, L. Bonechi, M. Bongi, A. Caputo, R. Ciaranfi, L. Cimmino, V. Ciulli, M. D'Errico, F. Giudicepietro, S. Gonzi, G. Macedonio, V. Masone, B. Melon, N. Mori, P. Noli, M. Orazi, P. Passeggio, R. Peluso, G. Saracino, L. Scognamiglio, P. Strolin, E. Vertechi, and L. Viliani. Volcanoes in italy and the role of muon radiography. https://royalsocietypublishing.org/doi/abs/10.1098/rsta.2018.0050, 2019.

[9] O. Catalano, M. Del Santo, T. Mineo, G. Cusumano, Maria Concetta Maccarone, and Giovanni Pareschi. Volcanoes muon imaging using cherenkov telescopes. https://www.sciencedirect.com/science/article/pii/S0168900215012772, 2016.

[10] M. Del Santo, O. Catalano, G. Cusumano, V. La Parola, G. La Rosa, M. C. Maccarone, T. Mineo, G. Sottile, D. Carbone, L. Zuccarello, G. Pareschi, and S. Vercellone. Looking inside volcanoes with the Imaging Atmospheric Cherenkov Telescopes. https://www.sciencedirect.com/science/article/pii/S0168900217302139, Dec 2017.

[11] D. Mollica, M. Del Santo, O. Catalano, R. Campana, T. Mineo, G. Cusumano, V. La Parola, M. C. Maccarone, G. La Rosa, and G. Sottile. Cherenkov muography for studying the internal structure of volcanoes. https://ui.adsabs.harvard.edu/abs/2018AGUFMNS23B0712M, Dec 2018.

[12] G. Vacanti, P. Fleury, Y. Jiang, E. Paré, A. C. Rovero, X. Sarazin, M. Urban, and T. C. Weekes. Muon ring images with an atmospheric Čerenkov telescope. https://www.sciencedirect.com/science/article/pii/0927650594900124, 1994.

[13] H. J. Völk and K. Bernlöhr. Imaging very high energy gamma-ray telescopes. https://doi.org/10.1007/s10686-009-9151-z, Aug 2009.

[14] G. Contino, O. Catalano, G. Sottile, P. Sangiorgi, M. Capalbi, G. Osteria, V. Scotti, H. Miyamoto, C. Vigorito, M. Casolino, and C. De Donato. An ASIC front-end for fluorescence and Čerenkov light detection with SiPM for space and ground applications. https://www.sciencedirect.com/science/article/pii/S0168900220309074, 2020.